

# Investigation of the effects of tissue material on the energy spectrum from Bebig Co-60 High Dose Rate Brachytherapy source based on the Monte Carlo simulation

N. Qomariyah<sup>1</sup>, F. Haryanto<sup>1\*</sup>, A. Waris<sup>1</sup>, R. Wirawan<sup>2</sup>

<sup>1</sup>Department of Physics, Faculty of Mathematics and Natural Science, Institut Teknologi Bandung, Jl. Ganesha 10 Bandung 40132, Indonesia

<sup>2</sup>Department of Physics, Faculty of Mathematics and Natural Science, University of Mataram, Jl. Majapahit 62 Mataram 83125, Indonesia

## ABSTRACT

### ► Original article

#### \*Corresponding author:

Dr. Freddy Haryanto,

E-mail: [freddy@itb.ac.id](mailto:freddy@itb.ac.id)

Received: October 2023

Final revised: March 2024

Accepted: June 2024

Int. J. Radiat. Res., January 2025;  
23(1): 97-102

DOI: 10.61186/ijrr.23.1.97

**Keywords:** Energy spectrum, Co-60, HDR brachytherapy, Monte Carlo.

**Background:** High Dose Rate (HDR) brachytherapy is an internal radiation therapy method that delivers high-intensity radiation at >12 Gy/hour dose rate. In clinical practice, the dose calculation is often carried out using the TG-43. However, the method does not consider the effects of patient dimensions and tissue heterogeneity. To overcome this challenge, this study proposed the use of energy spectrum analysis of the source model used. **Materials and Methods:** GEANT4 Monte Carlo simulation was used to build the geometry of Bebig Co-60 A86 source and radiation interaction system. The interaction physics used Penelope with  $1.0 \times 10^8$  beam on. The scoring region was spherical with radius 20, 30, 40, and 50 cm as well as material variations of water, muscle, and bone. **Results:** The spectrum in Compton continuum scattering increased along with a reduction in radius and material density, while the opposite effect was observed at the photoelectric peak. The photoelectric peak ratio experienced 2.96 times increment when the radius of the muscle increased from 20 cm to 30 cm. In addition, the particle count experienced an increment as the radius and medium density of the scoring region increased, with linear regression values of 0.83 for bone and 0.91 for the water and muscle. **Conclusion:** Increasing the radius and medium density led to variations in the height of the energy spectrum in Compton continuum and photoelectric regions. These variations caused an 18.42% increase in particle count when transitioning from 20 cm to 30 cm radius in water.

## INTRODUCTION

Brachytherapy (BT) is a type of radiation therapy that placing a radioactive source near a tumor. In addition, it can be categorized into 3 distinct groups based on the dose rates, including low (0.4–2 Gy/hour), medium (2–12 Gy/hour), and high (12 Gy/hour) <sup>(1)</sup>. Several studies have shown that the increasing use of Co-60 radioisotopes in High Dose Rate (HDR) brachytherapy is primarily due to the relatively high energy, long half-life (5.27 years), and economics <sup>(2-6)</sup>. This indicates that it is important to characterize the geometry of Co-60 source to consider the interactions of emitted particles. The characterization and optimization process can consider the direction and orientation of the source, the energy source, and the medium characteristics where it is placed <sup>(7, 8)</sup>.

According to the recommendations of the American Association of Physicists in Medicine (AAPM), the standard method for determining clinical brachytherapy dose is the Task Group No. 43 (TG-43) formalism. The method was updated to

TG-43U1, with enhancements and improvements to deepen the understanding of the calculation guidelines. This update includes integrating a Monte Carlo simulation method and experiments to improve accuracy and effectiveness in the dose calculation <sup>(9)</sup>. Based on TG-43U1, the determination of the dose is often performed by placing a single source in the centre of an infinite homogeneous water sphere phantom. The condition is intended to provide sufficient dispersion to calculate patient dose distribution and simplify the calculation <sup>(10-12)</sup>. However, the accuracy is limited in an ideal water phantom, as it does not account for the effects of tissue heterogeneity (e.g., elemental composition and tissue density) as well as the impact of patient dimensions.

In brachytherapy dosimetry studies, the phantom dimensions factors and medium variations are crucial points that must be extensively considered. Several studies showed that the size and medium variation of the phantom had a significant influence on the final dose administered through TG-43U1 method <sup>(13-15)</sup>. In TG-43U1 method, the dose distribution around the

target source can be determined experimentally or using the simulation method as an input parameter in the treatment planning system (TPS) (11). The simulation method is typically aimed at optimization before calculation in irradiation. An essential and influential parameter that must be reviewed is the photon energy spectrum distribution, showing the energy absorption process in a material (12, 16, 17). According to previous studies, GEometry ANd Tracking (GEANT4) Monte Carlo simulation is an accurate computational method to predicting the dose distribution (18, 19). GEANT4 can be used to accurately estimate the dose of radiation therapy, particularly in complex and heterogeneous situations, such as tissue heterogeneity (4, 18, 20-22).

The novelty of this study is to understand the effect of material variation and the scoring region size on the obtained dose from the energy spectrum of Bebig Co0.A86 brachytherapy source. In addition, a simpler model was also used in computing the dose that was related to the scoring region size and tissue heterogeneity simultaneously. The results obtained can help in the development of more accurate models of dose calculations.

**MATERIALS AND METHODS**

**GEANT4 simulation setup**

This study used Monte Carlo simulation calculations based on the GEometry ANd Tracking (GEANT4) GEANT4 version 9.5. In addition, GEANT4 toolkit was written in object-oriented C++ programming language to simulate the passage of particles through the material. The simulation input comprised Co-60 as an active radiation source consisting of two-photon energies, namely 1.173 MeV and 1.332 MeV. The distribution of Co-60 radiation was performed uniformly in a tube-shaped active core with a length of  $L = 3.5$  mm to obtain the energy spectrum distribution in the scoring region. The number of beams on particles was  $1.0 \times 10^8$  particles, and the characteristics of the radiation environment resembled the properties of water, muscle, and bone.

The photon interaction used in this study was a Penelope that occurred between photons and matter, comprising photoelectric, scattering (Compton scattering and Rayleigh scattering), and pair production. In addition, data visualization and analysis were carried out using ROOT version 5.34 program to determine the distribution of the photon energy spectrum.

**Modeling and description of Co0.A86 source**

Bebig Co0.A86 source model (Eckert & Ziegler Bebig GmbH, Germany) was used as HDR-BT Co-60 source. The geometrical specifications and materials of the source were based on the manufacturer's data. Geometry and material details are presented in figure

1. In addition, the radioactive Co-60 used in HDR-BT Co-60 source was contained in a cylindrical active core with a 0.5 mm diameter and an effective length of 3.5 mm. An air shell 0.1 mm thick, a density of  $0.0012 \text{ g/cm}^3$ , and with a conical tip, surrounded the active core. This core was also enclosed by a 0.15 mm thick stainless-steel capsule with an outside diameter of 1 mm. Cables were used in the simulation, with the source cable having a diameter of 0.9 mm and a length of 5 mm. Stainless steel materials were used for capsules and cables. The density of the materials used in this study was  $8.9 \text{ g/cm}^3$  for Co-60, stainless steel  $8.03 \text{ g/cm}^3$  for capsules, and  $4.81 \text{ g/cm}^3$  for cables.

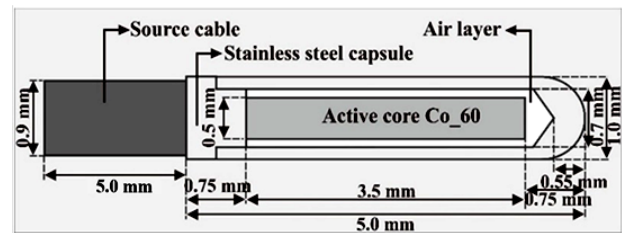


Figure 1. Schematic model of Bebig Co0.A86 source simulated in GEANT4 (size not to scale).

Table 1. Materials composition of the simulation materials (2).

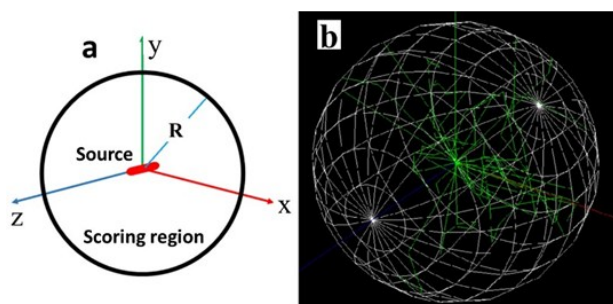
Element	Material (per cent weight)			
	Cobalt	Stainless-Steel	Water	Air
H	-	-	11.01	0.073
C	-	0.03	-	0.012
N	-	0.1	-	75.032
O	-	-	88.9	23.608
Si	-	0.75	-	-
P	-	0.045	-	-
S	-	0.03	-	-
Ar	-	-	-	1.274
Cr	-	17.0	-	-
Mn	-	2.0	-	-
Fe	-	65.543	-	-
Ni	-	12.0	-	-
Mo	-	2.5	-	-
Co	100.0	-	-	-
Density (g/cm <sup>3</sup> )	8.9	8.03/4.81	0.998	0.0012

Table 1 shows information about the materials' density and composition used in the source geometries. The chemical compositions of both water and air were derived from TG-43U1. In addition, stainless-steel composition was derived by averaging accepted parameters from AISI 316L alloy.

**Scoring region modeling**

The energy distribution of HDR-BT Co-60 source spectrum was calculated using a water phantom with spherical scoring regions (figure 2) of varying radius, including 20 cm, 30 cm, 40 cm, and 50 cm. The scoring region with a 50 cm radius was chosen as the ideal scoring region based on Tg-43U1 protocol. In these calculations, the water medium consisted of 2 atoms of hydrogen along with an oxygen atom, having a mass density of  $0.998 \text{ g/cm}^3$  at a temperature of  $22 \text{ }^\circ\text{C}$ . In addition to varying the size

of the scoring region, this study also explored variations in the scoring region medium for muscle and bone materials. The simulation model of the spectrum distribution in the assessment area was implemented using GEANT4, as presented in figure 2.



**Figure 2.** The geometry of energy spectrum calculation model with HDR-BT Co-60 source: **a)** Schematic model; **b)** GEANT4 visualization with particle trajectories.

The radius variation aimed to observe changes in the scoring region volume on the source spectrum, while the scoring region variation was carried out to investigate the impact of body tissue heterogeneity on the source spectrum pattern. Geometry and source characteristics of HDR-BT Co-60 were simulated in water phantoms, muscle and bone tissue phantoms separately using the same calculation mechanism as in the water medium. The simulated phantoms' chemical composition and density (weight fraction) were based on the International Commission on Radiation Units and Measurements (ICRU) report No. 44, as shown in table 2.

**Table 2.** Medium composition and density of the various phantoms in this study <sup>(8)</sup>.

Medium	Element composition (percent weight)										Density (g/cm <sup>3</sup> )	
	H	C	N	O	Na	Mg	P	S	Cl	K		Ca
Water	11.01	-	-	88.9	-	-	-	-	-	-	-	0.998
Muscle	10.2	14.3	3.4	71.0	0.1	-	0.2	0.3	0.1	0.4	-	1.050
Bone	3.4	15.5	4.2	43.5	0.1	0.2	10.3	0.3	-	-	22.5	1.920

### Spectrum energy distribution analysis

The simulation data provided information on the photon distribution at each energy tracked in the scoring region. The data analysis was processed using ROOT version 5.34 to generate spectrum distribution curves of Co-60 source and total particle counts in the scoring region. In addition, the changes in the spectrum distribution curves in Compton continuum, Compton edge, and photoelectric peak drop regions were analyzed. The changes in Compton continuum scattering and the photoelectric peak were represented by the heights of the curves at various sizes of the scoring region radius in each medium used. Theoretically, the ratio was compared with XCOM data based on the equality of mass attenuation coefficients. Furthermore, changes in photoelectricity were carried out on the ratio of photoelectric peak changes at the primary energy of Cobalt (1.173 MeV and 1.332 MeV). The parameter to be compared was the number of particle entries in each radius and

material's variation in scoring region. The number of entries showed how the radiation particle interacted in a volume-scoring region.

### Statistical analysis

A one-way ANOVA statistical test was used for statistical analysis, using SPSS software for Windows (IBM SPSS version 26.0). This test aimed to justify the effect of tissue material variation and the scoring region size on the resulting HDR-BT Co-60 source spectrum. The process of determining significant differences was performed by comparing the p-value of the test with the pre-set significance level. When the p-value was less than the pre-set significance level, it was possible to conclude that there was a significant difference between groups.

## RESULT

### The effect of radius scoring region

The energy spectrum distribution of Bebig Co0.A86 HDR source was obtained from simulations performed by GEANT4. The scoring region model was spherical with four radius variations of 20 cm to 50 cm in increments of 10. This radius size variation aimed to reveal the effect of patient dimensions. In addition, three variations of tissue heterogeneity were used in each scoring region size using water, muscle, and bone mediums. The distribution curves of the spectra at various radius sizes are presented in figure 3.

The energy spectrum distribution of Bebig Co0.A86 source at various radius sizes showed the same pattern. The spectrum distribution consisted of three regions, including Compton continuum region at energy 0 MeV to Compton edge (1.117 MeV), Compton edge at energies 1.117 MeV and 1.277 MeV, and photoelectric peaks at specific energies of 1.173 MeV and 1.332 MeV. In this study, the energy spectrum distribution model of Bebig Co0.A86 source had the same spectrum curve pattern as Sahoo *et al.* (2010) <sup>(23)</sup>. Variations in the scoring region radius size generally did not change the spectrum shape and pattern. The difference examined was in the height of the particle count, which affected the energy stored in the scoring region.

In Compton continuum scattering region, the smaller the radius of the scoring region, the higher the spectrum, where the difference in curve width narrowed as the energy increased. This occurred in all mediums used in the simulation. Meanwhile, the photoelectric peak showed a different pattern, where the spectrum curve increased as the radius of the scoring region increased, and was visible in the water and muscle medium. The ratios of the increase in the number of relative particles for each interval in the water medium at the peak energy of 1.173 MeV were 2.81, 1.23, and 1. For the peak energy of 1.332 MeV,

the ratios obtained were 3.13, 1.40, and 1. The increase ratio was 1 for a radius of 40 cm to 50 cm, showing that the photoelectric coincided. These results indicated that there was no difference in the height of the photoelectric peaks. For the medium muscle, the increased ratios were 2.59, 1.13, and 1 for 1.173 MeV energy and 2.96, 1.24, and 1 for 1.332 MeV energy, respectively. In the bone medium, the difference in curve width was significant at various radius sizes in Compton continuum scattering region. The results also showed that there was no variation in the height of the photoelectric peak at various radius sizes used.

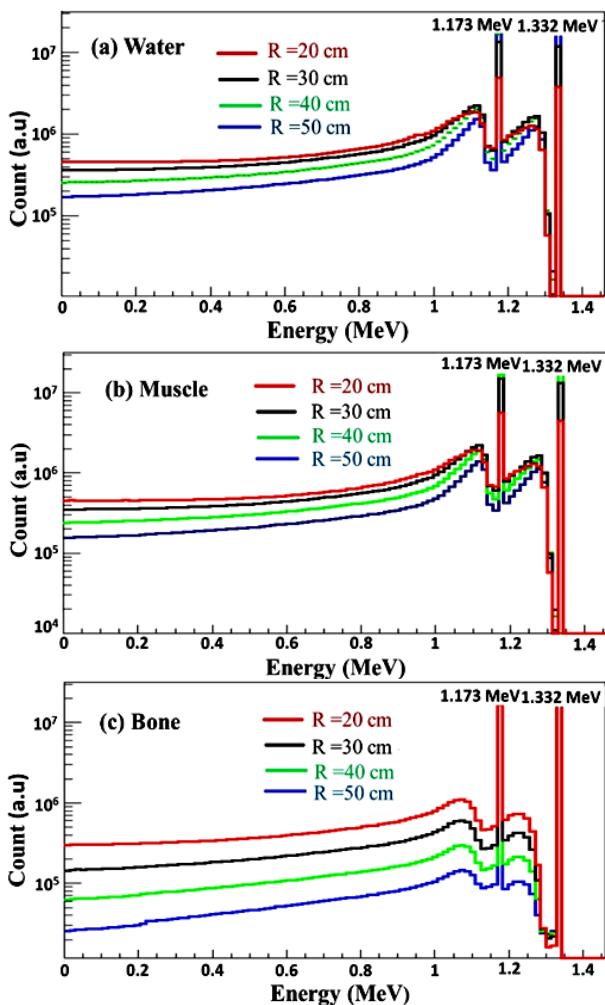


**Figure 3.** Energy spectrum distributions of HDR-BT Co-60 with GEANT4 in the scoring region in the medium of **a)** water, **b)** muscle, and **c)** bone.

The variation of the scoring region radius also led to differences in the total particle entries in the scoring region. Particle entries showed the number of radiation particle interactions in the scoring region. The simulation results indicated that the larger the size of the scoring region, the larger the total particle count. The total count was also impacted by the medium used, where the higher the density of the medium, the higher the total particle count. Total particle counts at various scoring region sizes are presented in figure 4.

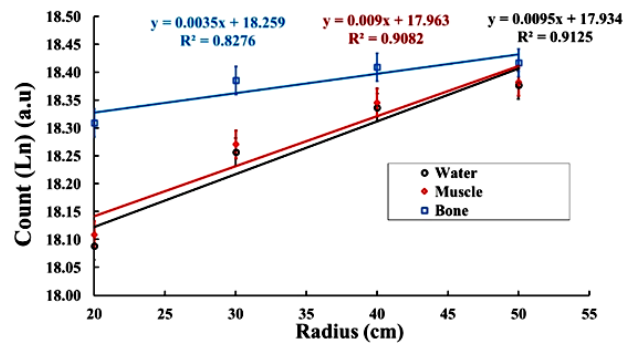


**Figure 4.** Comparison of the number of photons at various radius (20, 30, 40, and 50) cm of the scoring region for water, muscle, and bone (Point represents simulation data, while the line represents linear regression).

The simulation results in Figure 4 also reveal that the larger the radius of the scoring region, the higher the number of photon counts. The increase in the number of enumerations sloped down as the size of the scoring region increases. Furthermore, the increase in counts as the radius increased was 18.42%, 8.28%, and 4.08% in water, 17.61%, 7.77%, and 3.74% in muscle, and 7.95% and 2.40% in bone medium. The lowest increase of 0.76% was observed at a 40 cm to 50 cm radius. The results also indicate that the difference in the number of count of particles in the medium of bone and muscle against water decreased as the radius of the scoring region increased. The variation in the number of count in muscle and bone against water as a reference medium for a radius of 20 cm (smallest radius) was 2.07% and 24.73%, respectively. The increment observed decreased at a radius size of 50 cm (biggest radius), which was 0.56% and 4.10%. The effect of particle size on the scoring region size was also shown from the linear regression values of 0.83 for bone and 0.91 for water and muscle medium. ANOVA statistical analysis showed that the group mean test results indicated the effect of variations in the medium and the size of the scoring region on the distribution of the energy spectrum from HDR-BT Co-60 source. The obtained significance levels were 0.025 and 0.043, respectively, indicating significant differences as the P-values fell below the significance level of  $\alpha = 0.05$ .

Based on the results, there was a corresponding gradient of particle increase in water, muscle, and bone, namely 0.0095, 0.0090, and 0.0035, respectively. These gradient values correlated with the linear attenuation coefficients at the average energy of Co-60 (1.25 MeV) for water, muscle, and bone, namely  $0.063 \text{ cm}^{-1}$ ,  $0.066 \text{ cm}^{-1}$ , and  $0.113 \text{ cm}^{-1}$ . Therefore, the variation in the size of the scoring region and the medium used affected the interaction of photons in the scoring region.

#### The effect of medium variation

Three medium variations were used in this study, including water as a reference recommended by

AAPM TG-43U1, the muscle with nearly the same density as water, while the bone was used because it had a reasonably high-density contact with water. The distribution curves of the spectra in various media of water, muscle, and bone are presented in figure 3, while the difference for count in each medium is shown in figure 5.

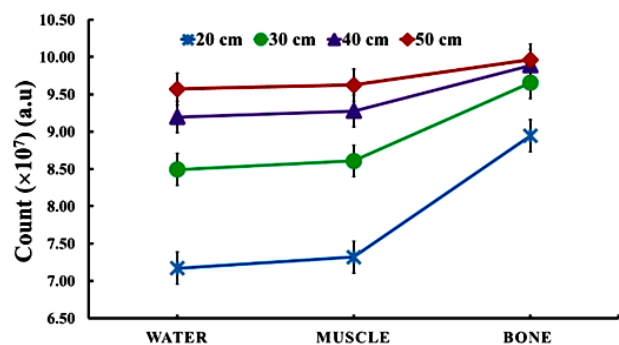


**Figure 5.** Increase in photon counts in water, muscle, and bone materials as the radius of the scoring region increases.

Compared to the scoring region radius variation, the medium variation did not change the distribution pattern of HDR-BT Co-60 source energy spectrum, but there was a difference in the spectrum height or the number of count (figure 3). The energy spectrum distribution in the muscle and bone medium had a spectrum distribution curve below the water spectrum curve for Compton continuum dispersion region. Furthermore, the muscle spectrum was nearly identical to water, where both mediums had similar density values. The bone medium had a lower spectrum height when compared to water, with the difference in curve width increasing as the radius-scoring region increased. In the scoring region with sizes of 20 cm and 30 cm, there was a difference in the height of the count at the photoelectric peak; the bone medium that had the highest photoelectric height. The particle number ratios for muscle and bone relative to water at a radius of 20 cm were 1.18 and 3.45 at the peak energy of 1.173 MeV and 1.19 and 4.33 for the energy of 1.332 MeV. The higher the radius of the scoring region, the smaller the ratio of the increase in the photoelectric peak of the medium to water, namely an average of 1.11 for muscle and 1.31 for bone at a radius of 30 cm. The ratio was 1 for a radius of 40 cm and 50 cm in the medium variation, indicating that the photoelectric peaks coincided. Figure 5 showed that the number of particles in each medium increased along with the radius of the scoring region. The bone medium with the highest density had the most significant number of count but the smallest increase in particle count occurred as the size of the scoring region increased.

## DISCUSSION

In this study, two main factors, namely the scoring

region size and tissue material, had been considered in HDR-BT Co-60 source particle interaction. The energy spectrum distribution of HDR-BT Co-60 source showed differences in the intensity of the spectrum curve in Compton continuum scattering region and the photoelectric peak. According to Moradi (2019), the tissue composition and density influenced Co-60 gamma energy spectrum, which determined the effective atomic number and electron density. Interactions at photon energies less than 1.022 MeV comprised Rayleigh scattering, photoelectricity, and Compton scattering. The probability of Rayleigh and photoelectric scattering decreased as the initial gamma-ray energy increased, while the probability of Compton scattering increased. In addition, these interactions interpret the characteristic gamma energy spectrum was formed by the complexity of the photon interaction with the medium, with a dynamic pattern based on the initial gamma-ray energies. The simulation results in Figure 4 depicts the highest particle counts occurring in the bone, indicating that particle interaction became more dominant in the bone medium. Meanwhile, low-density media tended to experience less angular deflection<sup>(17, 24-26)</sup>.

The size of the scoring region radius also affected the number of particle counts. The larger the size of the scoring region, the greater the number of particle counts. At a small radius (20 cm), it was concluded that as the space conditions were not sufficiently scattered, photon interactions were not fully recorded in the scoring region due to the limited volume size<sup>(27)</sup>. The increase in the number of photons count sloped down as the size of the scoring region increased (figure 4), following the theory underlying the Beer-Lambert Law. According to this law, radiation intensity drops exponentially with the thickness of the absorbing material. Based on Beer-Lambert Law, the intensity of radiation absorbed by the medium could be expressed as  $I_{absorption} = I_0(1 - e^{-\mu x})$ , where  $I_0$  represent the initial intensity,  $\mu$  is the linear absorption coefficient, and  $x$  is the scattering material thickness. The results showed why the particle count was sloping at large scoring regions. Particle interactions decreased with decreasing photon energy as the distance of the interaction medium increased. This study compared MC simulation results with theoretical mass attenuation coefficient data using XCOM data. The mass attenuation coefficient illustrated the ability of a material to absorb incident photon energy per unit mass. In addition, the mass attenuation coefficient was essential for understanding radiation interaction with material and predicting the radiation dose received by the tissue<sup>(25, 28-29)</sup>.

Tissue material and size of the scoring region must be considered when calculating brachytherapy doses. Several studies showed that tissue material could affect the spread and absorption of radiation,

and the scoring region provided space for radiation scattering.

## CONCLUSION

The energy spectrum distribution of Bebig Co0.A86 source showed Compton continuum region, Compton edges at energies of 1.117 MeV and 1.277 MeV, and photoelectric peaks at 1.173 MeV and 1.332 MeV. At smaller radius sizes, the spectrum of Compton scattering interactions increased, while the change in the photoelectric peak was higher as the radius of the scoring region became larger. The particle count increased by 18.42% when transitioning from a 20 cm to a 30 cm radius in water.

## ACKNOWLEDGEMENTS

None.

**Ethical consideration:** None.

**Author contributions:** Each author performed an equal contribution to the study design, collecting data and analysis, and manuscript writing.

**Conflict of interest:** The authors affirm that there are no conflicts of interest to declare.

**Funding:** The Indonesian Education Scholarship (BPI) of Kemendikbudristek of Indonesia, the Centre for Higher Education Fund (Balai Pembiayaan Pendidikan Tinggi), Education Fund Management Institute (LPDP), and Riset PPMI KK ITB 2023 supported this work.

## REFERENCES

1. Visser AG and Symonds RP (2001) Dose and volume specification for reporting gynaecological brachytherapy: time for a change. *Radiation and Oncology*, **58**(2001): 1-4.
2. Guerrero R, Almansa JF, Torres J, et al. (2014) Dosimetric characterization of the <sup>60</sup>Co BEBIG Co0.A86 high dose rate brachytherapy source using PENELOPE. *Phys Medica*, **30**(8): 960-96.
3. Almansa JF, Guerrero R, Torres J, et al. (2017) Monte Carlo dosimetric characterization of the Flexisource Co-60 high-dose-rate brachytherapy source using PENELOPE. *Brachytherapy*, **16**(5): 1073-1080.
4. Granero D, Prez-Calatayud J, Ballester F (2007) Technical note: Dosimetric study of a new Co-60 source used in brachytherapy. *Med Phys*, **34**(9): 3485-3488.
5. Joya M, Nedaie HA, Geraily G, et al. (2022) BEBIG <sup>60</sup>Co HDR brachytherapy source dosimetric parameters validation using GATE Geant4-based simulation code. *Heliyon*, **8**(3): e09168.
6. Campos LT and De Almeida CEV (2015) Monte Carlo dosimetry of the <sup>60</sup>Co BEBIG high dose rate for brachytherapy. *PLoS One*, **10**(9): 1-9.
7. Elboukhari S, Yamni K, Ouabi H, et al. (2020) Technical note: Dosimetric study for the new BEBIG <sup>60</sup>Co HDR source used in brachytherapy in water and different media using Monte Carlo N-Particle eXtended code. *Appl Radiat Isot*, **159**: 109087.
8. Badry H, Oufni L, Ouabi H, et al. (2018) Monte Carlo investigation of the dose distribution for <sup>60</sup>Co high dose rate brachytherapy source in water and in different media. *Appl Radiat Isot* **136**: 104-

- 110.
9. Beaulieu L, Carlsson Tedgren A, Carrier JF, et al. (2012) Report of the Task Group 186 on model-based dose calculation methods in brachytherapy beyond the TG-43 formalism: Current status and recommendations for clinical implementation. *Med Phys*, **39**(10): 6208-6236.
10. Perez-Calatayud J, Ballester F, Das RK et al. (2012) Dose calculation for photon-emitting brachytherapy sources with average energy higher than 50 keV: Report of the AAPM and ESTRO. *Med Phys*, **39**(5): 2904-2929.
11. Rivard MJ, Coursey BM, DeWerd LA, et al. (2004) Update of AAPM Task Group No. 43 Report: A revised AAPM protocol for brachytherapy dose calculations. *Med Phys*, **31**(3): 633-674.
12. Wu J, Xie Y, Ding Z, Li F, et al. (2021) Monte Carlo study of TG-43 dosimetry parameters of GammaMed Plus high dose rate <sup>192</sup>Ir brachytherapy source using TOPAS. *J Appl Clin Med Phys*, **22**(6): 146-153.
13. Seo H, Haque M, Hill R, et al. (2009) Effect of varying phantom size in dosimetry of iridium-192: A comparison of experimental data with EGSnrc Monte Carlo calculation. *IFMBE Proc*, **25**(3): 396-399.
14. Ababneh E, Dababneh S, Wadi-Ramahi S, et al. (2018) Physics elements of an algorithm for brachytherapy dose calculation in homogeneous media for <sup>192</sup>Ir source. *Radiat Phys Chem*, **149**: 90-103.
15. Schoenfeld AA, Harder D, Poppe B, et al. (2015) Water equivalent phantom materials for <sup>192</sup>Ir brachytherapy. *Phys Med Biol*, **60**(24): 9403-9420.
16. Akar Tarim U, Gurler O, Ozmutlu EN, et al. (2012) The energy spectrum of 662keV photons in a water equivalent phantom. *Radiat Phys Chem*, **81**(7): 745-748.
17. Moradi F, Khandaker MU, Alrefae T, et al. (2018). Monte Carlo simulations and analysis of transmitted gamma ray spectra through various tissue phantoms. *Appl Radiat Isot*, **146**: 120-126.
18. EL Bakkali J, Doudouh A, Mansouri H (2018) Assessment of Monte Carlo Geant4 capabilities in prediction of photon beam dose distribution in a heterogeneous medium. *Phys Med*, **5**: 1-5.
19. Ababneh E, Dababneh S, Qatarneh S, et al. (2014) Enhancement and validation of Geant4 Brachytherapy application on clinical HDR <sup>192</sup>Ir source. *Radiat Phys Chem*, **103**: 57-66.
20. Ab Shukor NS, Musarudin M, Abdullah R, et al. (2020) Effects of different volumes of inhomogeneous medium to the radial dose and anisotropy functions in HDR brachytherapy. *J Phys Conf Ser*, **1497**(1): 691-708.
21. Grevillot L, Frisson T, Maneval D, et al. (2011) Simulation of a 6 MV Elekta Precise Linac photon beam using GATE/GEANT4. *Phys Med Biol*, **56**(4): 903-918.
22. Dehghan ABY, Mostaar A, Azadeh P (2023). Implementation of geant4 application for tomography emission Monte Carlo Code in the calculation of dose distribution in external radiation therapy. *Int J Radiat Res*, **21**(4): 663-673.
23. Sahoo S, Selvam TP, Vishwakarma RS, et al. (2011). Monte Carlo modeling of 60 Co HDR brachytherapy source in water and in different solid water phantom materials. *Jour of Med Phys*, **35**(1): 15-22.
24. Bozkurt A and Sengul A (2021) Monte Carlo approach for calculation of mass energy absorption coefficients of some amino acids. *Nucl Eng Technol*. **53**(9): 3044-3050.
25. Mann-Krzisnik D, Verhaegen F, Enger SA (2018) The influence of tissue composition uncertainty on dose distributions in brachytherapy. *Radiation Oncology*, **126**(3):394-410.
26. Bechchar R, Senhou N, Ghassoun J (2019) A fast and accurate analytical method for 2D dose distribution calculation around brachytherapy sources in various tissue equivalent phantoms. *Int J Radiat Res*, **17**(4): 531-540.
27. Ahmed SN (2007) Physics and Engineering of Radiation Detection: First edit. Academic Press is an imprint of Elsevier, Netherlands.
28. Fotina I, Zourari K, Lahanas V, et al. (2011) A comparative assessment of inhomogeneity and finite patient dimension effects in <sup>60</sup>Co and <sup>192</sup>Ir high-dose-rate brachytherapy. *J Contemp Brachytherapy*, **10**(1): 73-84.
29. Jashni, Hojatollah Karimi, Safigholi H, et al. (2015) Influences of spherical phantom heterogeneities on dosimetric characteristics of miniature electronic brachytherapy X-ray sources: Monte Carlo study. *Appl Radiat Isot*, **95**:108-113.